7th International Conference on Computational and Mathematical Biomedical Engineering - CMBE2021
27–29 June 2022, Italy
P. Nithiarasu and C. Vergara (Eds.)

GENERATION OF ARTIFICIAL RETINAL MICROVASCULAR NETWORKS: VIRTUAL POPULATIONS FOR *IN SILICO* TRIALS

Rémi Hernandez[1,2,3], Savita Madhusudhan[3,4], Yalin Zheng[1,3,4], and Wahbi K. El-Bouri[1,2,3]

[1]Liverpool Centre for Cardiovascular Science, University of Liverpool and Liverpool Heart & Chest Hospital, Liverpool, UK
[2]Department of Cardiovascular and Metabolic Medicine, University of Liverpool, Liverpool, UK
[3]St. Paul's Eye Unit, Royal Liverpool University Hospital, Liverpool, UK
[4]Department of Eye and Vision Science, University of Liverpool, UK

SUMMARY

Defects in the oxygen supply to the retina are a common cause of several retinal diseases. The inner retinal vasculature can be imaged noninvasively and numerous quantitative vascular biomarkers have been suggested for certain diseases. However, the links between vascular alterations and the development of pathologies are not yet clear. We propose a method to generate microvascular networks that can be used to create populations of retinas, differentiated by a handful of metrics. This work will enable further *in silico* simulations that will shed light on the relationship between microvasculature and cellular functions.

Key words: *constructive constrained optimisation, macula, artificial vascular network*

1 INTRODUCTION

Human retina has high metabolic activity and, consequently, a high oxygen consumption rate. In addition, retinal vasculature is constrained spatially so as not to interfere with visual processing. As a result, a fragile balance exists between the inflow of nutrients and the metabolic consumption. A number of retinal diseases, such as age-relate macular degeneration and diabetic retinopathy are caused by an alteration of this balance in the central part of the retina, the macula. The macula is particularly sensitive to alterations in the vascular perfusion system due to its high density of photoreceptor cells.

The vasculature embedded in the inner retinal layers is one of the two pathways of oxygen delivery to retinal tissue - the other being the choriocapillaris. Conveniently, retinal microvasculature can be imaged *in vivo* and non-invasively using optical coherence tomography angiography (OCTA). However, we currently lack ways to relate microvascular biomarkers with oxygen distribution inside the tissue.

Computational models can help solve these issues. However, computation of intraluminal blood flow requires fully connected representations of capillary networks, while current automated segmentation techniques are limited to larger venules and arterioles. Earlier computational studies have investigated blood flow in artificial retinal vasculature [8]. However, these works rely on idealised representations of the vasculature, with strong assumptions on the symmetry of the vascular trees.

Algorithms such as the constructive constrained optimisation (CCO) grow artificial microvascular networks, introducing statistical variance between simulations that may help recreate the heterogeneity both within the retina and between subjects [9]. We propose here a method to construct artificial retinal capillary plexi using CCO based on an initial segmentation of larger arterioles and venules, as seen on en-face OCTA of the superficial vascular complex (SVC). The generated capillary networks are compared quantitatively to retinal images for validation.

Parameter	$N_{terms,1}$	$N_{terms,2}$	FAZ width	Perifovea width	f_n	ε	θ_{min}	δ	γ
Value	1500	500	$0.4\,\mathrm{mm}$	$2\,\mathrm{mm}$	5	10^{-4}	$8\pi/5$	0	2.85

Table 1: Parameters used for the simulations. $N_{terms,i}$: number of terminal vessel grown at stage i; f_n: factor to scale the size of the neighborhood of a candidate new vessel; ε: tolerance for the fixed point iteration; θ_{min}: minimum angle at bifurcation; δ: symmetry ratio; γ: Murray's law exponent.

2 METHODOLOGY

To generate vascular networks with realistic aspect, we manually segment larger arterioles and venules from an en-face OCTA scan. These vessels are specific to the SVC and can be straightforwardly differentiated from the more numerous capillaries. A CCO algorithm is then used to sprout the remaining vascular tree from the segmented vessels [9]. The algorithm picks a point at random within the domain to be perfused and links it to the current tree in a way that satisfies certain geometrical and haemodynamic constraints while minimising the biological cost of forming a vessel. More precisely, we use the 'sprouting cost function' proposed by Talou et al. with coefficients $(c_v, c_p, c_d) = (50, 0.5, 10^4)$ [9].

The perfusion domain in this work is a square with dimensions matching an OCTA field-of-view of $3 \times 3\,\mathrm{mm}^2$ centered on the fovea. Note that the algorithm requires one vascular segment as the root of the vascular tree, while the segmented vessels have no shared root within the perfusion domain. To tackle this issue, a non-branching tree surrounding the perfusion domain is manually created and linked to the segmented vessels, as shown on Figure 1. Following the nomenclature by Talou et al., these vessels are of the transport type and non-branching [9]. Three subdomains are defined: the perifovea, parafovea and the foveal avascular zone (FAZ). The peri- and parafovea are populated during separate stages, starting with the former, while the FAZ remains devoid of vessels. The location of the distal end of new vessels is drawn from a uniform distribution over the current stage's subdomain. For details of the subdomains, see Figure 1. New vessels are added to the tree until the required number of terminal vessels for the current stage have been added to the tree.

For the analysis, the trees are divided into subtrees containing all vessels with the same bifurcation number. This number is computed as the number of upstream bifurcations leading to a vessel. Vessels with a bifurcation number of 10 or more are categorized as capillaries and put in the same category. Mean and standard deviation of vessel diameter is computed for each group and compared with data from the literature. Additionally, each tree skeleton is visualized and exported as images using the VTK library. From the images, fractal dimension (FD) and intercapillary distance (ICD) are computed. Using skeleton maps of the vasculature, FD is computed using a box counting method and ICD using an euclidean distance transform, similarly to [5].
An emphasis is made on comparing with data from OCTA studies. However, given the limited number of comparable results from OCTA, studies based on different imaging means are also included. Along with FD and ICD, the metrics proposed by Chu et al. are used to characterise the vasculature [3]. Vessel area density (VAD) is the percentage of the total area occupied by vessels. The vessel perimeter index (VPI) is the ratio of the total vessel perimeter by the total area. The vessel diameter index (VDI) is the ratio of the total vessel area by the total vessel length. The vessel complexity index (VCI) is the ratio of the square of the total vessel perimeter by the total vessel area. The vessel skeleton density (VSD) is the ratio of the total vessel length by the total area. The metrics reported with pixel as a unit, namely, VSD, VPI and VDI are converted to $\mu\mathrm{m}$ using the approximation $1\ \mathrm{pixel} = 6.8\mu\mathrm{m}$

3 RESULTS

Simulations ($n = 50$) are run using the number of terminal vessels as a criteria for termination. The number of terminal vessels for each stages is chosen to achieve a mean intercapillary distance close to the value reported by Liu et al. [5]. Details of the parameters used in the simulations can be found in Table 1. The seed used to initiate the random number generator is set to be the time of the execution. An example of the output is shown in Figure 1. Visually, the artificial tree resemble the OCTA. However, one of the branches segmented from the OCTA does not sprout. This can be explained by the presence of concurrent branches nearby that start sprouting earlier in the process. As a consequence, the probability of a new point to link with that isolated branch is low [9].

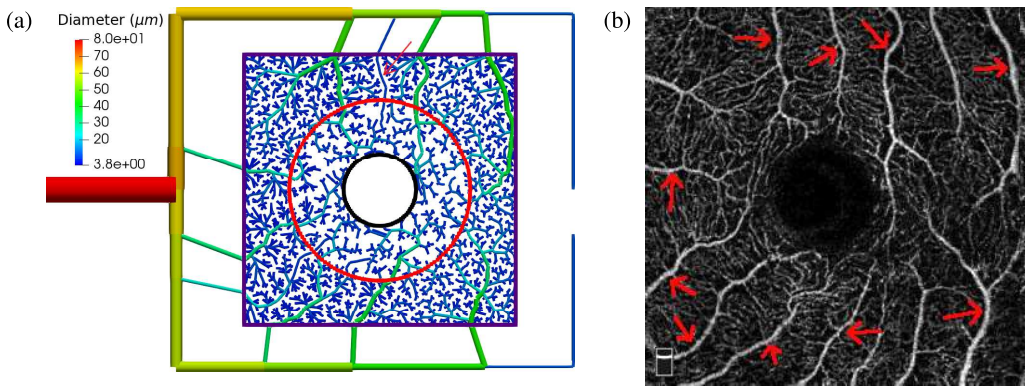

Figure 1: An example of the output vasculature from our method. (a) Vascular network generated with the constructive constrained optimisation. The colored line define the outline of the perifovea (purple) and parafoveal (red) areas that are perfused during the first and second stage, respectively. The FAZ is contained within the black circle. The arrow shows a root vessel that did not branch. Vessels outside of the perifoveal area are not included in any of the calculations and the FAZ is excluded from the total area. (b) An OCTA en-face image from the ROSE-1 dataset of the superficial vascular complex from which the largest vessels have been segmented to serve as a base for the tree branching algorithm (shown by the red arrows) [6].

	VAD	VDI (μm^{-1})	VCI	VSD (μm^{-1})	FD	ICD (μm)
Chu et al.	0.505 (0.01)	24.073 (0.64)	17962 (591)	0.0146 (0.004)	–	–
Other	0.482 (0.032) [1]	17 (0.09) [1]	–	–	1.45 [6] 1.68 [7]	22 [5]
This work	0.21 (0.001)	10.34 (0.05)	3389 (28)	0.02 (0.0001)	1.68 (0.001)	25.8 (0.3)

Table 2: Comparison of global vascular metrics between this work and values for control subjects reported in [1, 3, 5, 6]. Values reported as: *mean (standard deviation)*. VAD: vessel area density; VPI: vessel perimeter index; VDI: vessel diameter index; VCI: vessel complexity index; VSD: vessel skeleton density; FD: fractal dimension; ICD: mean intercapillary distance. For details, see [3].

Global vascular metrics are reported in Table 2 along with values from the literature. Fractal dimension for the generated trees is relatively constant and close to values reported for large field studies of the retina but higher than values for the macula only [7, 6]. Note that in both studies, the fractal dimension is computed on segmented images, either manually or automatically, therefore discarding data from some of the smaller caliber vessels which may impact the fractal aspect of the image. From the metrics proposed by Chu, VSD and vessel perimeter index (data not shown) are in close agreement to the study [3]. On the other hand, VAD, VDI and VCI are under the reported values by Chu and Alam. As VAD and VCI are computed on binarized vessel maps, we suspect that overestimates follow from the thresholding and binarization of OCTA images and that this increase might be two-fold.

Figure 2 shows geometrical aspects of the vessels categorised according to their bifurcation number.

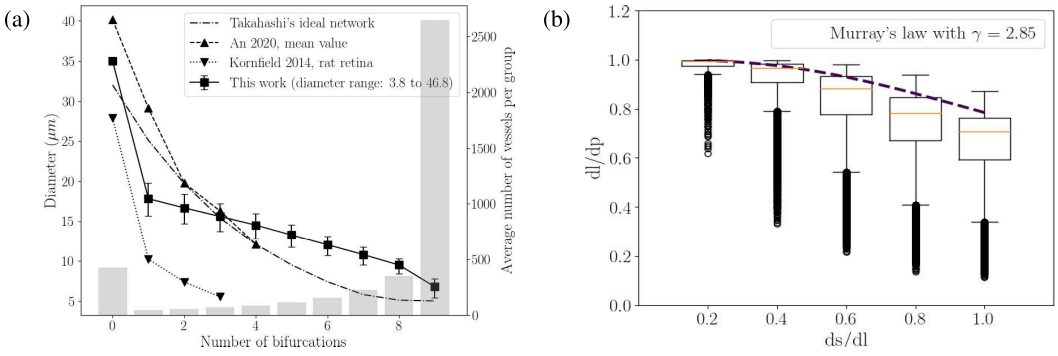

Figure 2: Geometrical aspect of the trees. (a) Diameter against bifurcation number and comparison with normal subject from the work of An, an ideal retinal vascular network proposed by Takahashi et al. and the study by Kornfield et al. on the rat retina [2, 4, 8]. Grey bars are the number of vessel counted in each group. (b) Branch ratios at bifurcation compared to theoretical values from Murray's law [8]. dl: largest daughter branch's diameter; ds: smallest daughter branch's diameter; dp parent's diameter.

When compared with data from experiments on donor eyes, the generated vessels are smaller in caliber for the first two groups [2]. The dimensions of the area of interest in the study are similar to those used in the simulations. However, one can see in Figure 1 from An et al.'s paper that two larger caliber vessels are included in the measurements which are not typically seen on a 3×3 mm^2 OCTA [2]. This could be due to the whole-mounting technique used in the study and could explain the larger caliber of the most upstream vessels. The generated vasculature matches the theoretical, ideal dichotomous tree proposed by Takahashi et al. [8] (Figure 2), both in diameter and in the bifurcation ratio. The overall trend for the diameter corresponds with reported trends from human and rat retinas alike.

4 CONCLUSIONS

We proposed a method to generate populations of superficial retinal vascular networks using an adaptation of the CCO algorithm. The resulting networks visually resemble vascular plexi observed with OCTA and some of the quantitative biomarkers computed on OCTA images. However, the metrics involving vessel area, such as VAD, are much larger on OCTA than on our generated trees. This is due in part to a fundamental aspect of OCTA scans which tends to overestimate the width of vessels. Indeed, capillaries in the macula have diameter of $5\,\mu\text{m}$–$10\,\mu\text{m}$ while OCTA has a spatial resolution of $10\,\mu\text{m}$–$20\,\mu\text{m}$. Furthermore, both Alam et al. and Chu et al. used a larger field of view: 6.72×6.72 mm^2 and 6×6 mm^2, respectively. Additionally, many of those metrics vary across imaging modalities, devices and segmentation strategy and their reproducibility is not always good.
Our method does not differentiate between arterial and venous trees. Indeed, the segmented vessels used as a root for further branching includes both arterioles and venules. We estimated that it was not necessary to differentiate both vessel types at this stage. Rather, by including as much information from the OCTA we hope to achieve a better fit with the metrics presented here.

In future work, we are planning to simulate populations of retinaes by using one or a combination of the metrics presented here (e.g., ICD) as a termination criterion for the algorithm. We seek to generate vascular networks that recreate key characteristics of real retinal microvasculatures. These networks will then be coupled with mathematical models of intravascular and extravascular transport to simulate oxygen perfusion within a population of virtual retinaes. We will use these models to shed light on the relationships between the microvasculature and cellular functions in the retina.

REFERENCES

[1] M. Alam, Y. Zhang, J. I. Lim, R. V. Chan, M. Yang, and X. Yao. Quantitative oct angiography features for objective classification and staging of diabetic retinopathy. *Retina (Philadelphia, Pa.)*, 40:322–332, 2020.

[2] D. An, P. Yu, K. B. Freund, D. Y. Yu, and C. Balaratnasingam. Three-dimensional characterization of the normal human parafoveal microvasculature using structural criteria and high-resolution confocal microscopy. *Investigative Ophthalmology & Visual Science*, 61:3–3, 8 2020.

[3] Z. Chu, J. Lin, C. Gao, C. Xin, Q. Zhang, C.-L. Chen, L. Roisman, G. Gregori, P. J. Rosenfeld, and R. K. Wang. Quantitative assessment of the retinal microvasculature using optical coherence tomography angiography. *Journal of Biomedical Optics*, 21:066008, 6 2016.

[4] T. E. Kornfield and E. A. Newman. Regulation of blood flow in the retinal trilaminar vascular network. *Journal of Neuroscience*, 34:11504–11513, 8 2014.

[5] K. Liu, Y. Guo, Q. You, T. Hormel, T. S. Hwang, and Y. Jia. Normative intercapillary distance and vessel density data in the temporal retina assessed by wide-field spectral-domain optical coherence tomography angiography. *Experimental Biology and Medicine*, 246:2230–2237, 10 2021.

[6] Y. Ma, H. Hao, J. Xie, H. Fu, J. Zhang, J. Yang, Z. Wang, J. Liu, Y. Zheng, and Y. Zhao. Rose: A retinal oct-angiography vessel segmentation dataset and new model. *IEEE Transactions on Medical Imaging*, 40: 928–939, 2021.

[7] B. R. Masters. Fractal analysis of the vascular tree in the human retina. *Annual Review of Biomedical Engineering*, 6:427–452, 7 2004.

[8] T. Takahashi, T. Nagaoka, H. Yanagida, T. Saitoh, A. Kamiya, T. Hein, L. Kuo, and A. Yoshida. A mathematical model for the distribution of hemodynamic parameters in the human retinal microvascular network. *Journal of Biorheology*, 23:77–86, 2009.

[9] G. D. M. Talou, S. Safaei, P. J. Hunter, and P. J. Blanco. Adaptive constrained constructive optimisation for complex vascularisation processes. *Scientific Reports 2021 11:1*, 11:1–22, 3 2021.